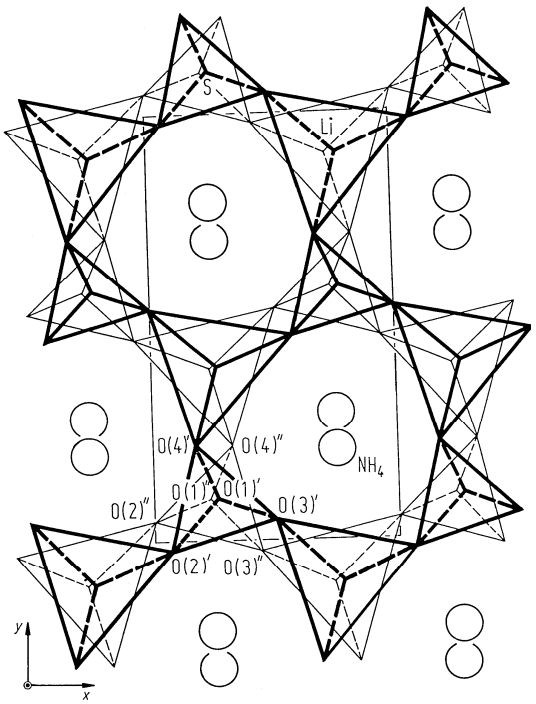

Fig. 41A-5-001. NH_4LiSO_4. Structure of phase I [81Ito]. Arrangement of SO_4 and LiO_4 tetrahedra viewed along *c*. The thick lines with primed O atoms and the thin lines with double-primed O atoms are fractional pairs in the disordered state. The primed O atoms are referred in Table 41A-5-001 and Table 41A-5-002.

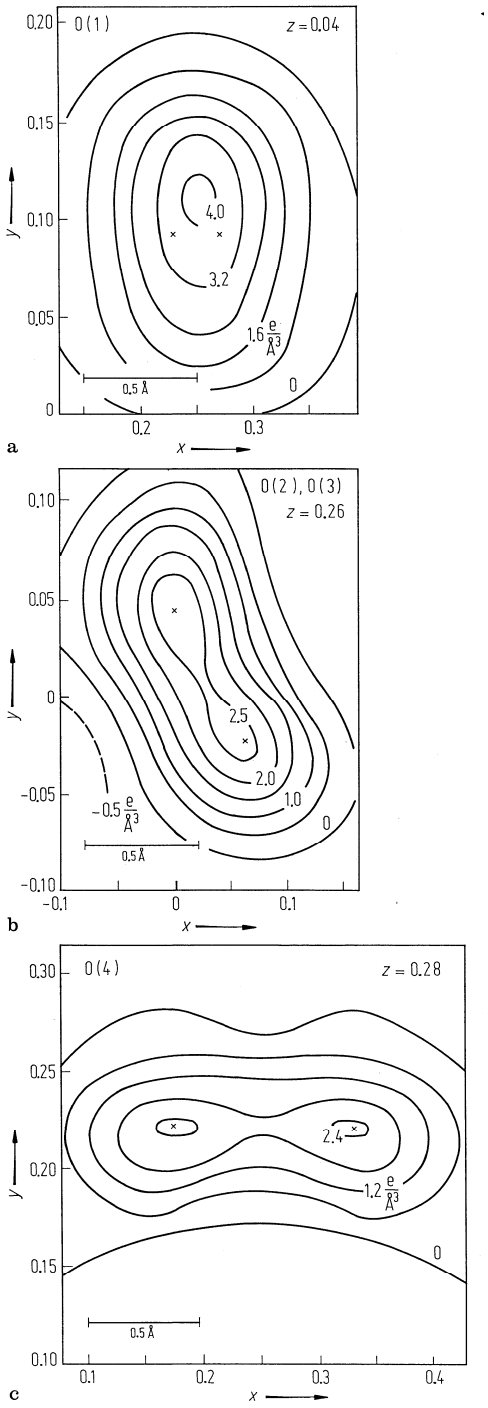

Fig. 41A-5-002. NH_4LiSO_4. Structure of phase I [81Ito]. Electron density maps [e/Å^3] around oxygen atoms, showing the disordered state. $T = 478$ K. (**a**) O(1), (**b**) O(2), O(3), (**c**) O(4).

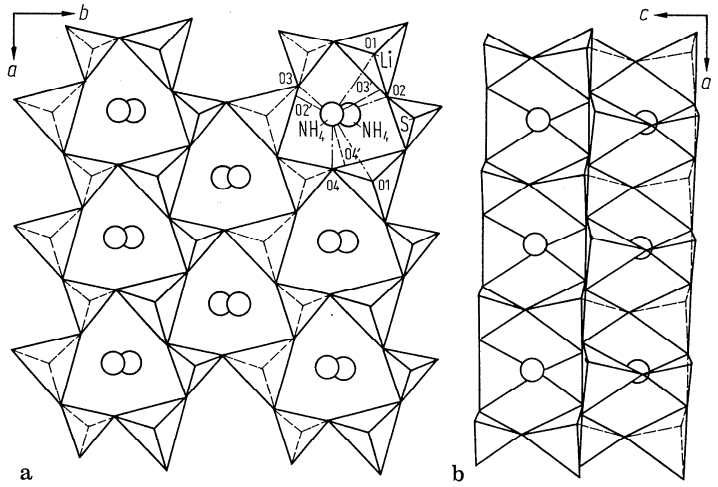

Fig. 41A-5-003. NH_4LiSO_4. Structure of phase II [69Dol]. Views of polyhedral linkage. (**a**) along the *c* axis. Only one tetrahedral layer is shown. In successive layers, which are almost exactly eclipsed in this view, a LiO_4 tetrahedron pointing up is replaced by a SO_4 tetrahedron pointing down, etc. Fractional coordinates (*z*) of labeled atoms are NH_4 0.50 and 0.00, O(1) 0.51, O(2) 0.25, O(2′) 0.75, O(3) 0.26, O(3′) 0.76, O(4) 0.27, O(4′) 0.77, Li 0.32, S 0.30. (**b**) along the *b* axis is showing "double chain" of tetrahedra.

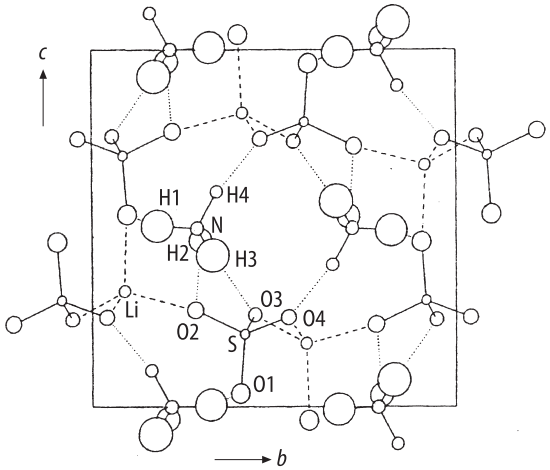

Fig. 41A-5-004. NH_4LiSO_4. Structure of phase II [93Mas]. T = 298 K. Projection along the *a* axis. Broken and dotted lines indicate the nearest Li–O pairs and O–H pairs, respectively.

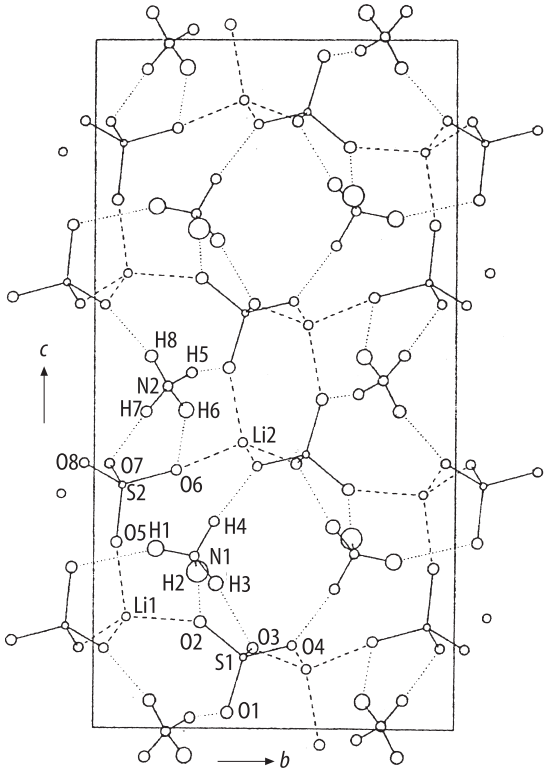

Fig. 41A-5-005. NH_4LiSO_4. Structure of phase III [93Mas]. T = 190 K. Projection along the a axis. Broken and dotted lines indicate the nearest Li–O pairs and O–H pairs, respectively.

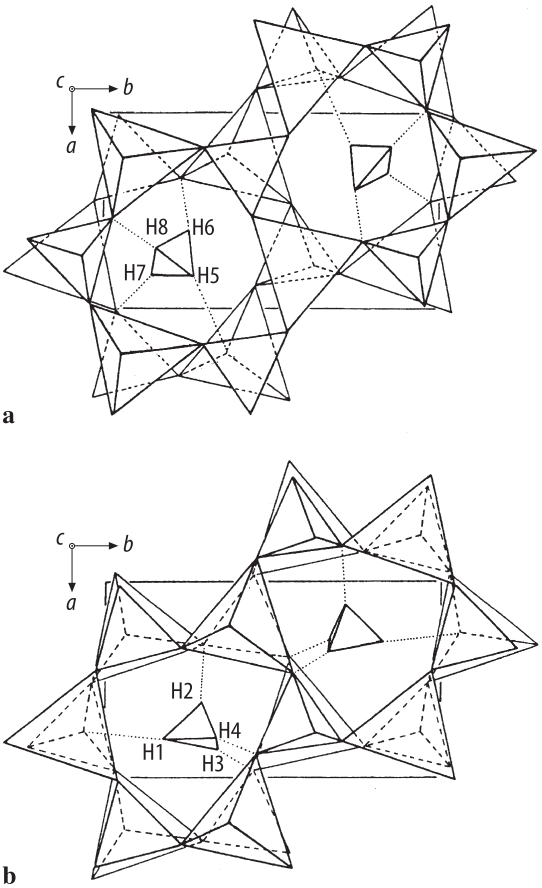

Fig. 41A-5-006. NH_4LiSO_4. Structure of phase III [93Mas]. T = 190 K. Pseudohexagonal networks viewed along the c axis. (**a**) $1/4 < z < 3/4$, (**b**) $0 < z < 1/2$. Large, middle and small tetrahedra are LiO_4, SO_4 and NH_4, respectively. Hydrogen bonds are denoted by dotted lines.

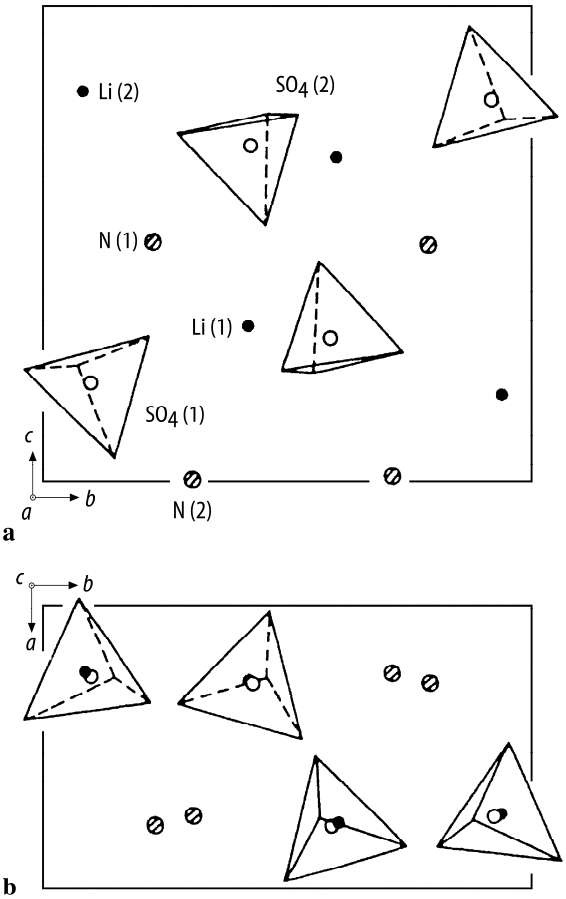

Fig. 41A-5-007. NH_4LiSO_4. Structure of phase VI [94Has]. p = 9.5·10^8 Pa. T = RT. Projection (**a**) along the a axes, (**b**) along the c axes.

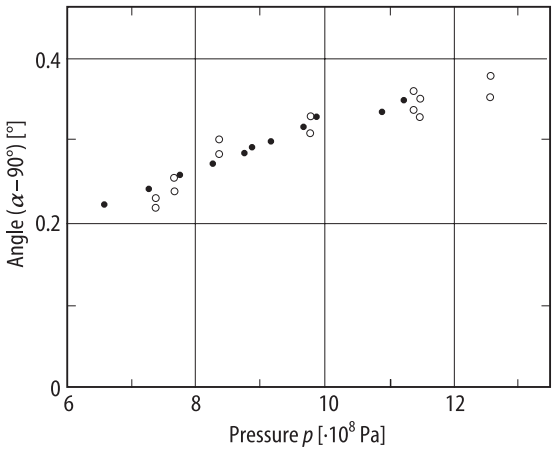

Fig. 41A-5-008. NH_4LiSO_4. (α–90°) vs. p [94Has]. T = RT. α: monoclinic angle. Two kinds of pressure medium were employed; ethanol (full circle) and kerosene (open circle).

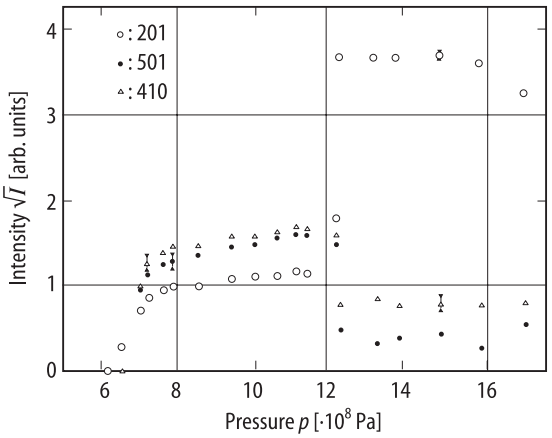

Fig. 41A-5-009. NH_4LiSO_4. $\sqrt{I}$ vs. p [94Has]. T = RT. I: X-ray diffraction intensity.

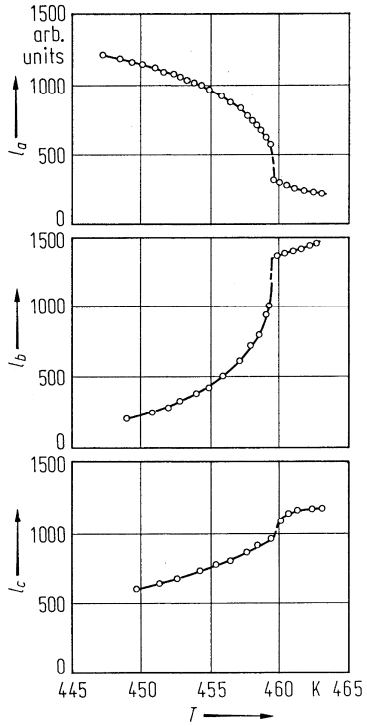

Fig. 41A-5-010. NH_4LiSO_4. l_a, l_b, l_c vs. T [77Isk]. l_a, l_b, l_c: linear thermal expansion along the a, b, c axes, respectively.

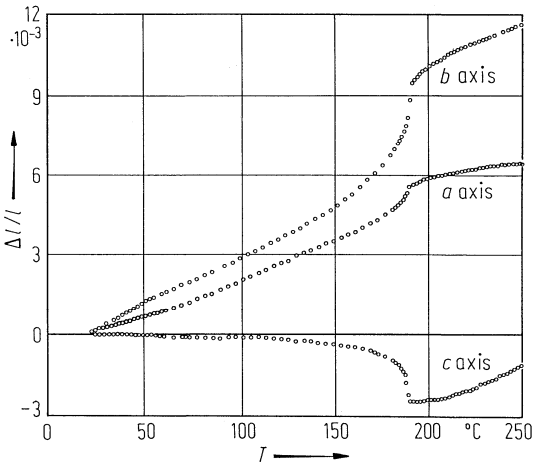

Fig. 41A-5-011. NH_4LiSO_4. Δ*l*/*l* vs. *T* [81Hir]. Δ*l*/*l*: linear thermal expansion.

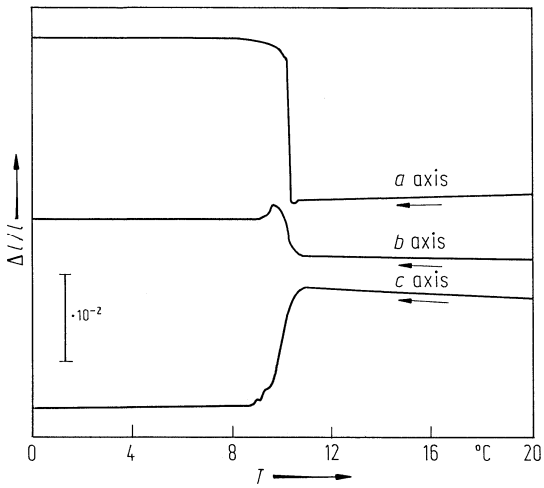

Fig. 41A-5-012. NH_4LiSO_4. Δ*l*/*l* vs. *T* [80Shi]. Δ*l*/*l*: linear thermal expansion.

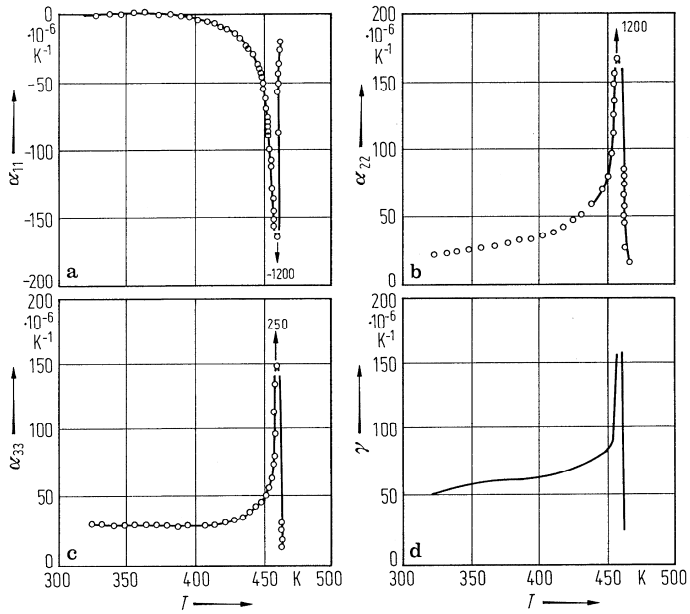

Fig. 41A-5-013. NH_4LiSO_4. α_{11}, α_{22}, α_{33}, γ vs. T [77Isk]. γ: cubic thermal expansion coefficient.

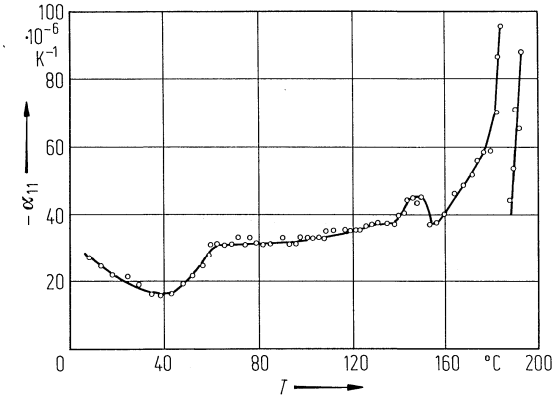

Fig. 41A-5-014. NH_4LiSO_4. α_{11} vs. T [82Sha]. α_{11}: linear thermal expansion coefficient along the *a* axis.

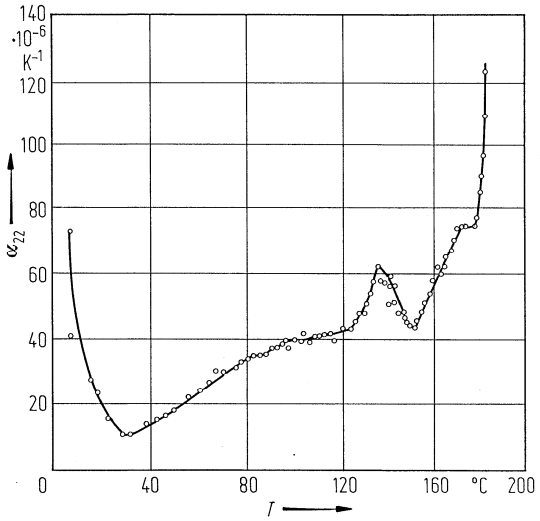

Fig. 41A-5-015. NH_4LiSO_4. α_{22} vs. T [82Sha]. α_{22}: linear thermal expansion coefficient along the b axis.

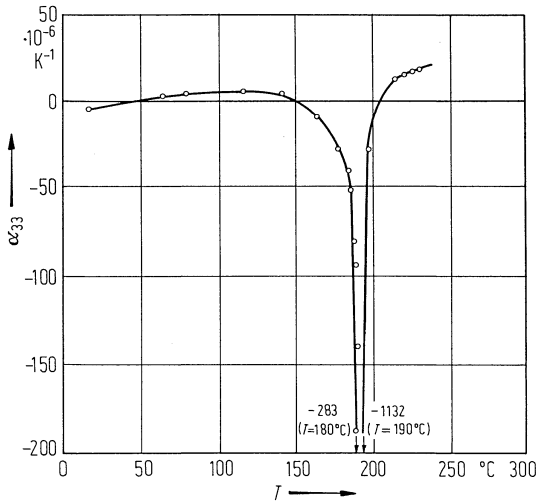

Fig. 41A-5-016. NH_4LiSO_4. α_{33} vs. T [82Sha]. α_{33}: linear thermal expansion coefficient along the c axis. Note that Fig. 41A-5-013 is due to $Pnc2_1$.

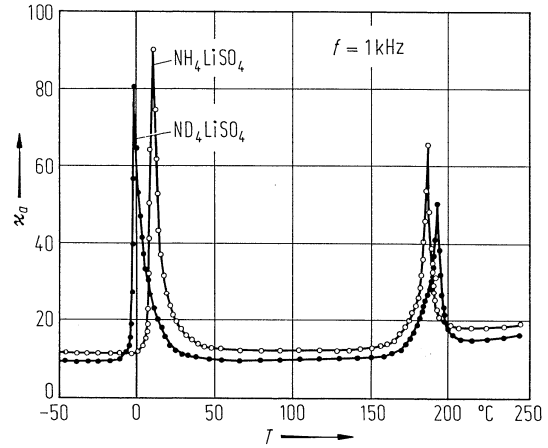

Fig. 41A-5-017. NH_4LiSO_4, ND_4LiSO_4. κ_a vs. T [82Sum]. f = 1 kHz.

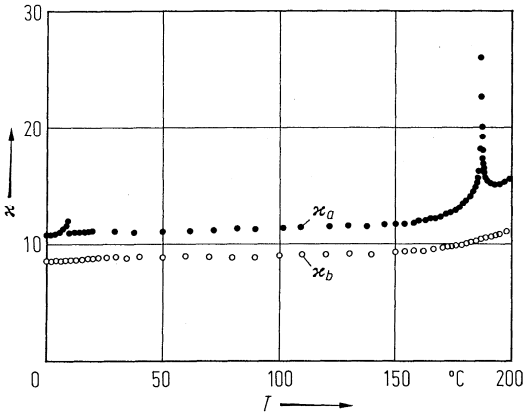

Fig. 41A-5-018. NH_4LiSO_4. κ_a, κ_b vs. T [75Mit]. f = 3 kHz.

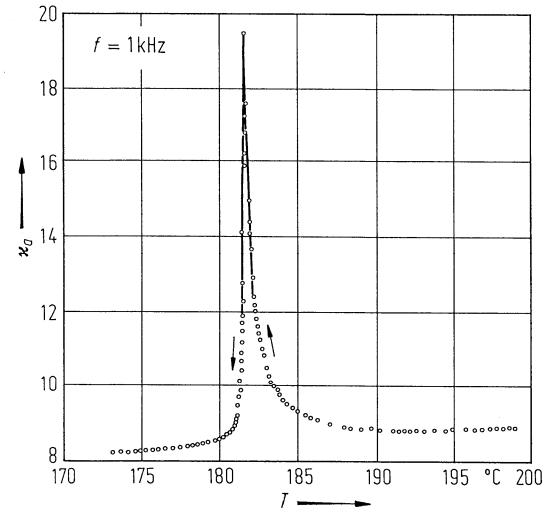

Fig. 41A-5-019. NH_4LiSO_4. κ_a vs. T [86Ani].

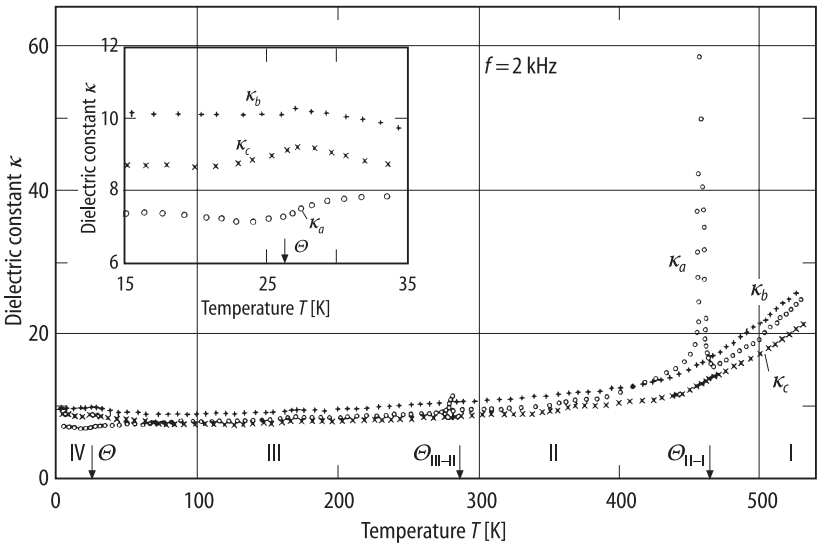

Fig. 41A-5-020. NH_4LiSO_4. κ_a, κ_b, κ_c vs. T [88Smu]. $f = 2$ kHz.

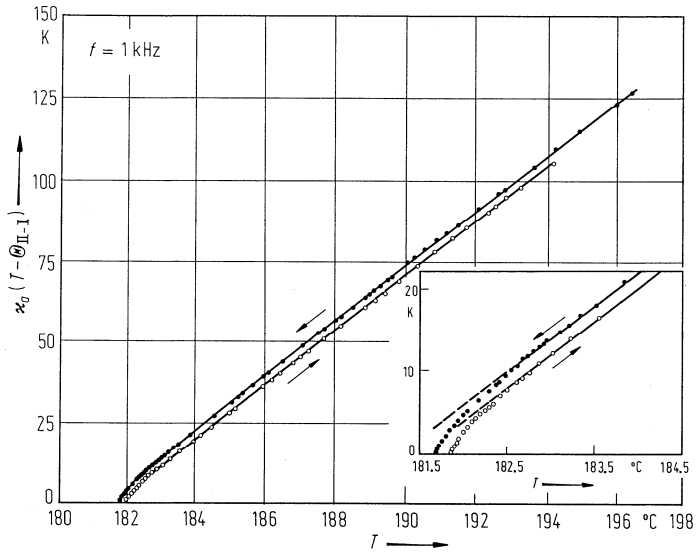

Fig. 41A-5-021. NH_4LiSO_4. $\kappa_a(T - \Theta_{II-I})$ vs. T [86Ani].

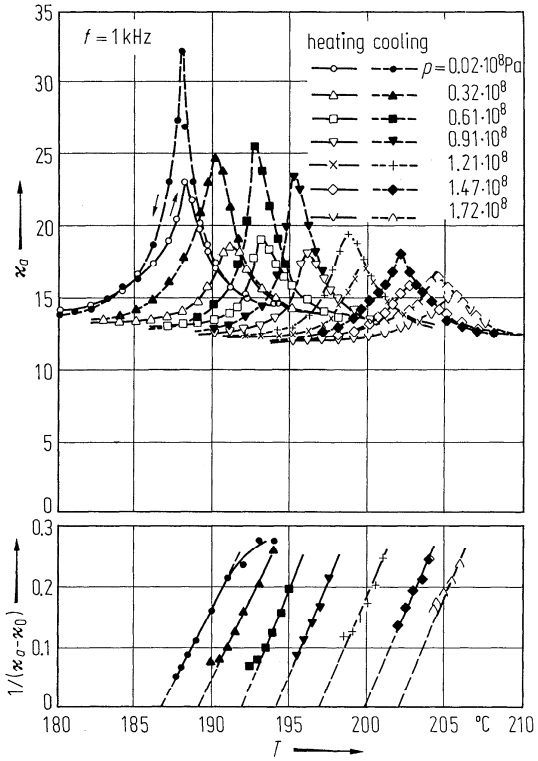

Fig. 41A-5-022. NH_4LiSO_4. κ_a, $1/(\kappa_a - \kappa_0)$ vs. T [77Shi]. Parameter: p. $\kappa_0 = 10.9$ (κ_0 is the value of the flat part of κ_a at 50 °C).

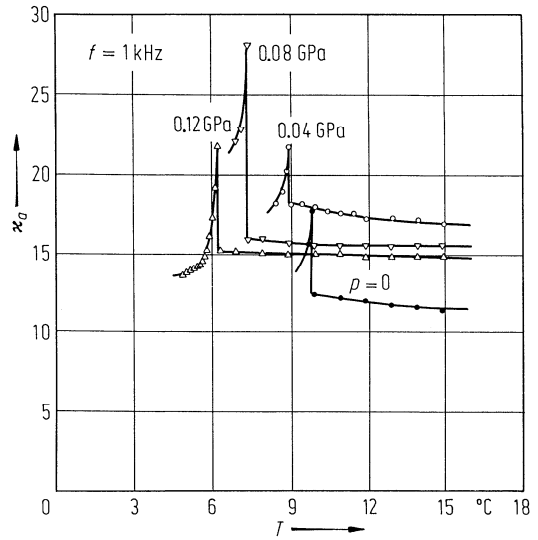

Fig. 41A-5-023. NH_4LiSO_4. κ_a vs. T [80Shi]. Parameter: p. On cooling.

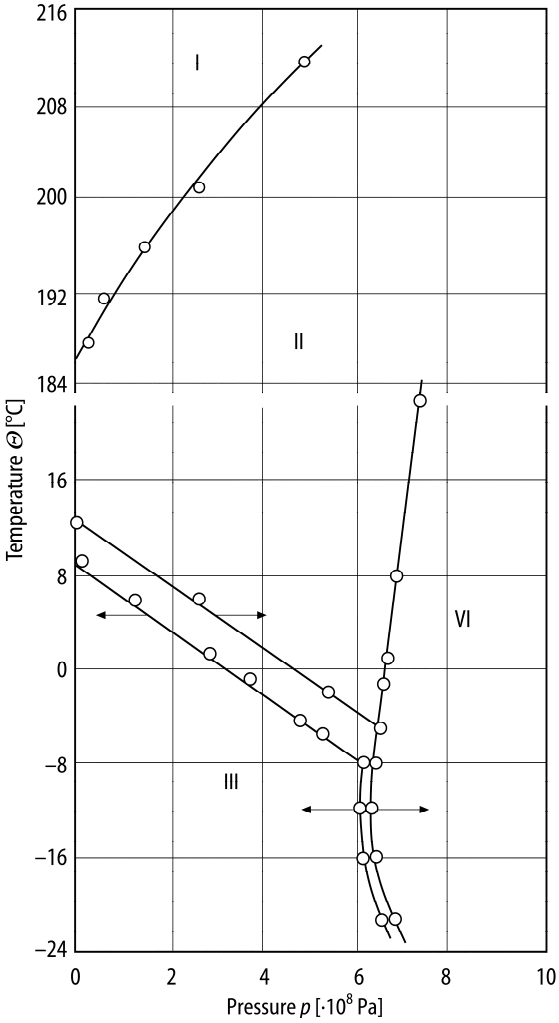

Fig. 41A-5-024. NH_4LiSO_4. Θ vs. p [77Che].

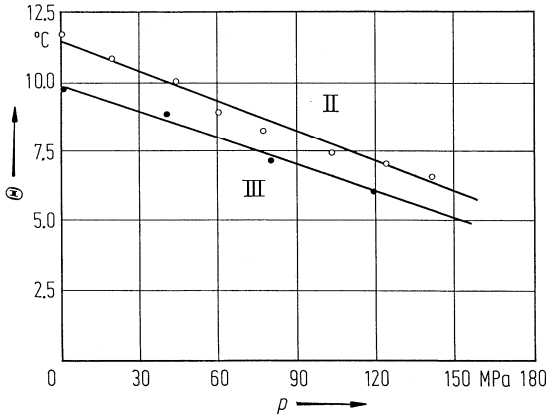

Fig. 41A-5-025. NH_4LiSO_4. Θ vs. p [80Shi]. Open circle: from DTA (on heating), full circle: from κ_a (on cooling).

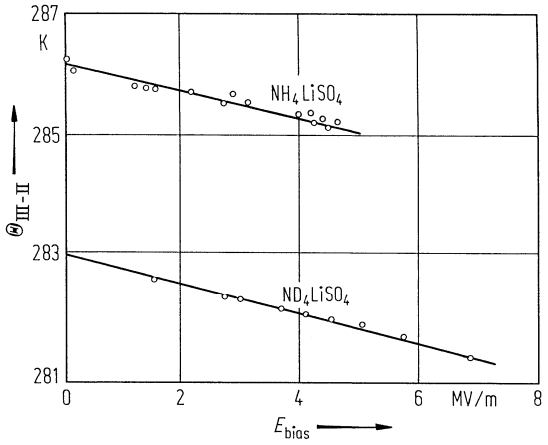

Fig. 41A-5-026. NH_4LiSO_4, ND_4LiSO_4. Θ_{III-II} vs. E_{bias} [84Smu]. On cooling.

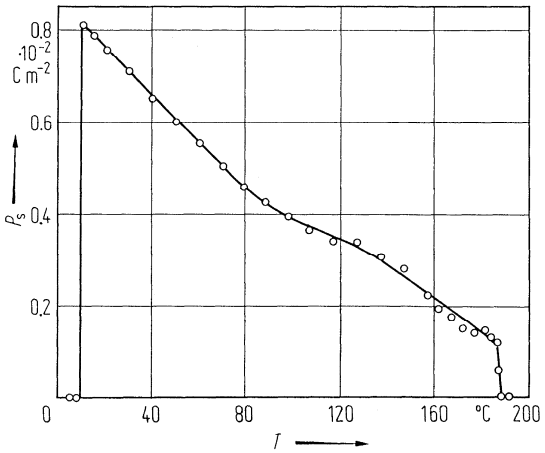

Fig. 41A-5-027. NH_4LiSO_4. P_s vs. T [75Mit].

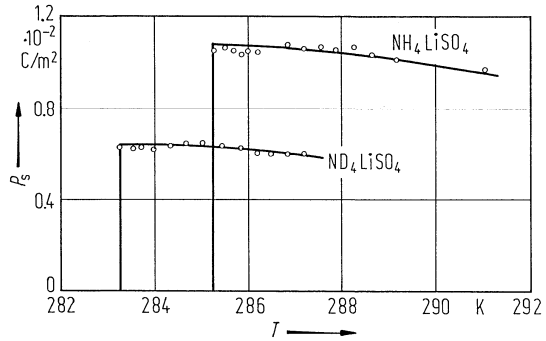

Fig. 41A-5-028. NH_4LiSO_4, ND_4LiSO_4. P_s vs. T in the vicinity of Θ_{III-II} [84Smu]. On cooling.

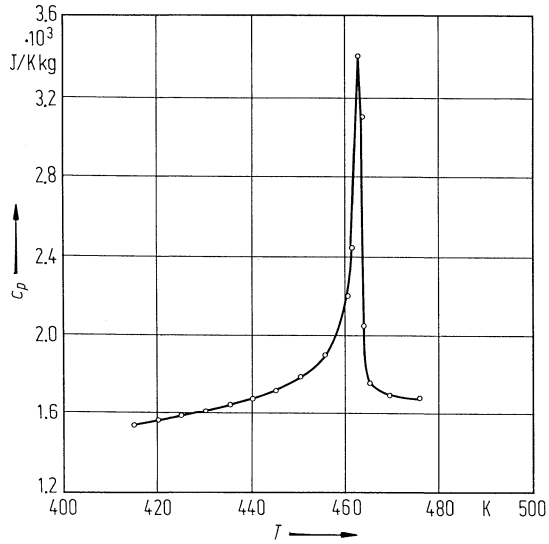

Fig. 41A-5-029. NH_4LiSO_4. c_p vs. T [80Loi]. c_p: specific heat capacity at constant pressure.

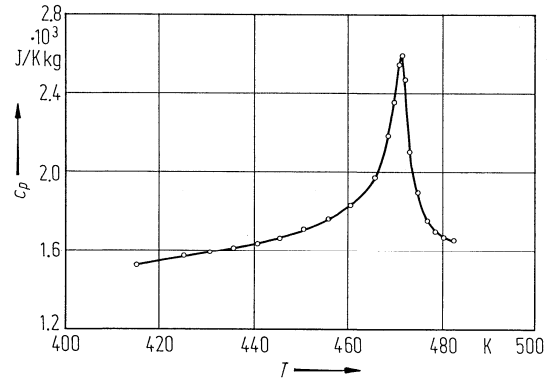

Fig. 41A-5-030. ND_4LiSO_4. c_p vs. T [80Loi]. c_p: specific heat capacity at constant pressure.

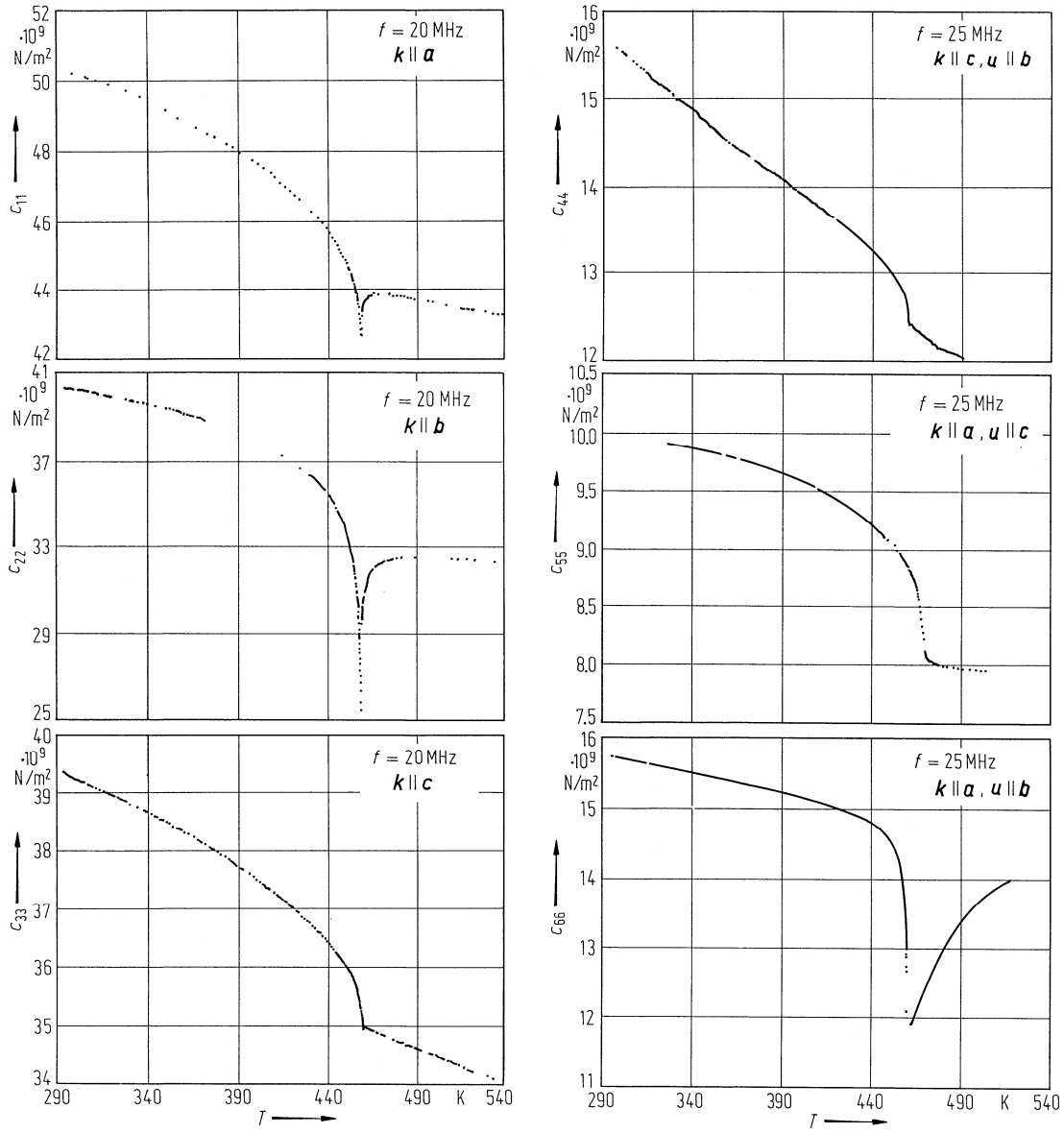

Fig. 41A-5-031. NH_4LiSO_4. $c_{\lambda\mu}$ vs. T [86Wys]. ***k***: wave vector, ***u***: polarization (displacement) vector.

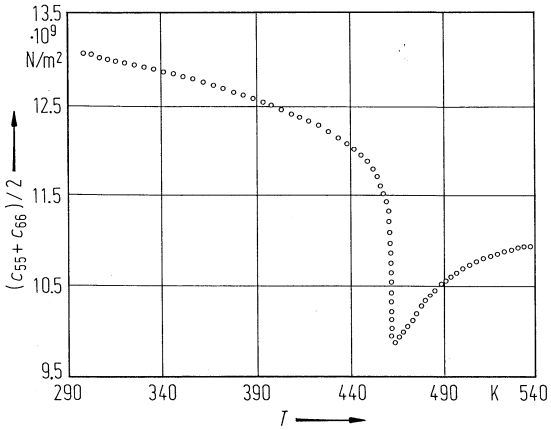

Fig. 41A-5-032. NH_4LiSO_4. $(c_{55} + c_{66})/2$ vs. T [87Sch1]. Measured by Brillouin scattering.

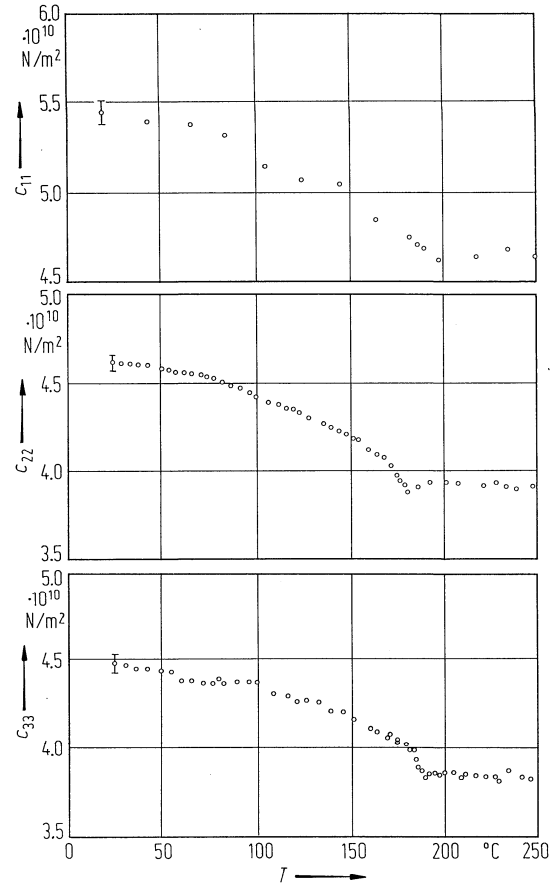

Fig. 41A-5-033. NH_4LiSO_4. $c_{\lambda\lambda}$ vs. T [81Hir]. $c_{\lambda\lambda}$: elastic stiffnesses measured by Brillouin scattering.

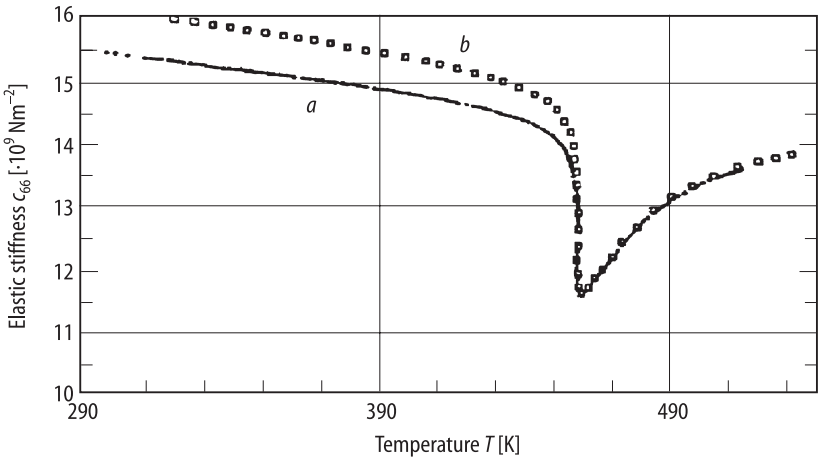

Fig. 41A-5-034. NH_4LiSO_4. c_{66} vs. T [87Sch1]. c_{66}: elastic stiffnesses. Curve *a* measured by ultrasonic method at $10 \cdot 10^6$ Hz, *b* calculated by Brillouin scattering on $(c_{44} + c_{66})/2$ and c_{44}.

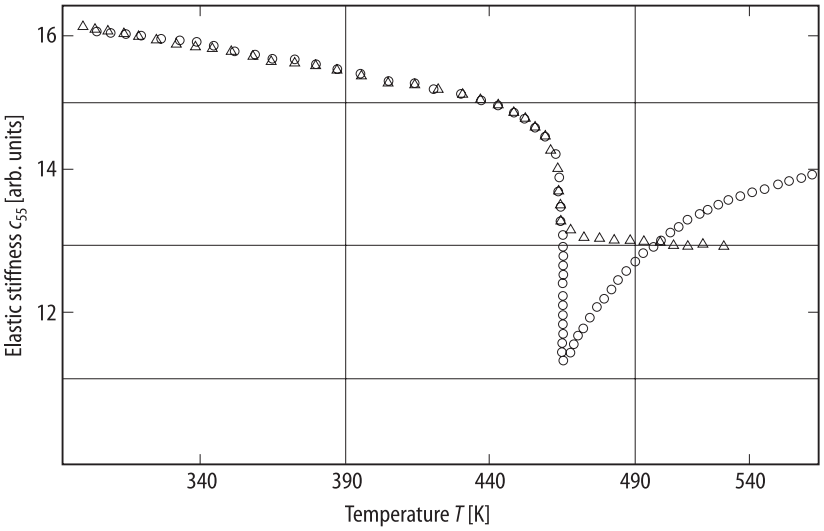

Fig. 41A-5-035. NH_4LiSO_4. c_{55} vs. T [87Sch2]. c_{55}: elastic stiffnesses measured by ultrasonic method at $25 \cdot 10^6$ Hz (open circle), by Brillouin scattering nearly at $10 \cdot 10^9$ Hz (open triangle).

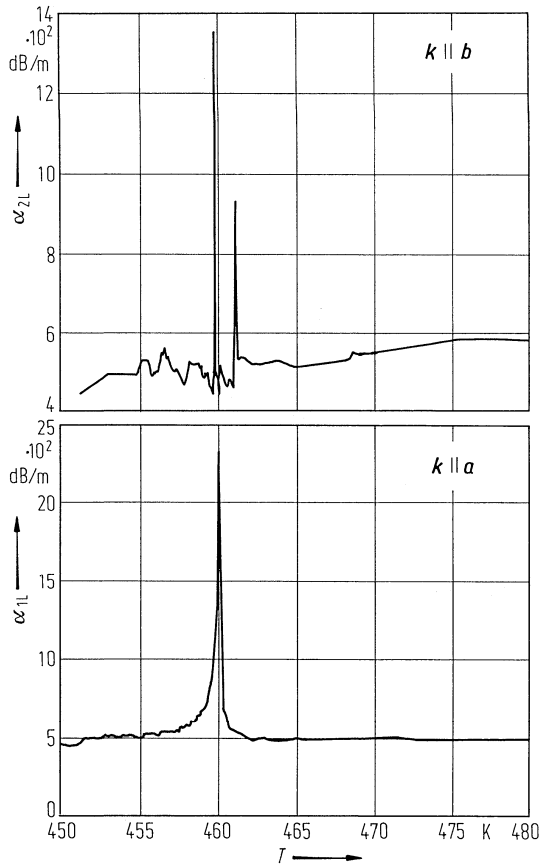

Fig. 41A-5-036. NH_4LiSO_4. α_{1L} and α_{2L} vs. T [86Wys]. α_{1L}, α_{2L}: attenuation coefficient of longitudinal ultrasonic wave. $f = 20$ MHz.

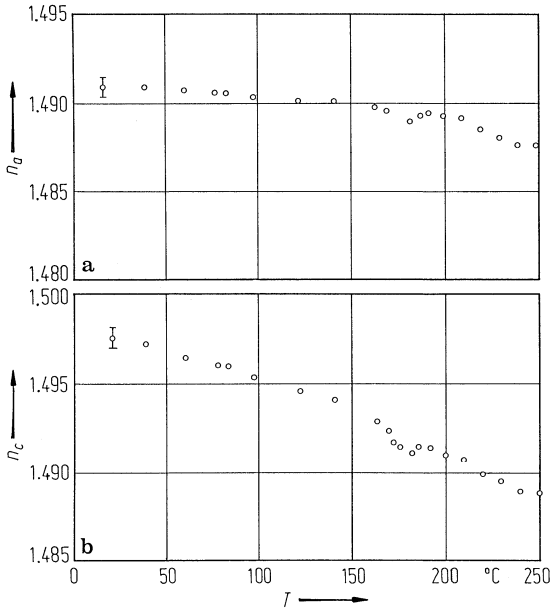

Fig. 41A-5-037. NH_4LiSO_4. n_a, n_c vs. T [81Hir]. (**a**) n_a, (**b**) n_c. $\lambda = 632.8$ nm.

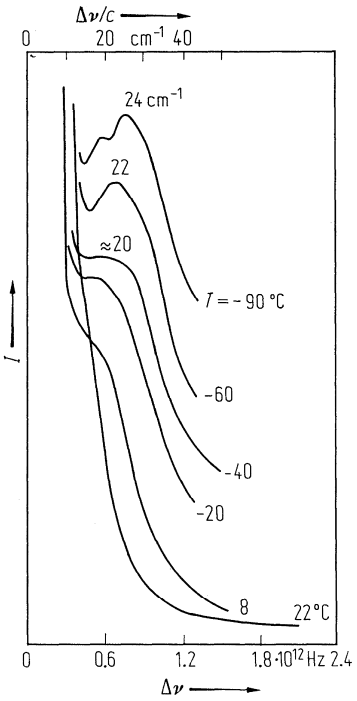

Fig. 41A-5-038. NH_4LiSO_4. I vs. $\Delta\nu$ [77Pou]. I: Raman scattering intensity of the lowest frequency mode in the scattering geometry of $X(YX)Y$. $\Delta\nu$: frequency shift. Parameter: T.

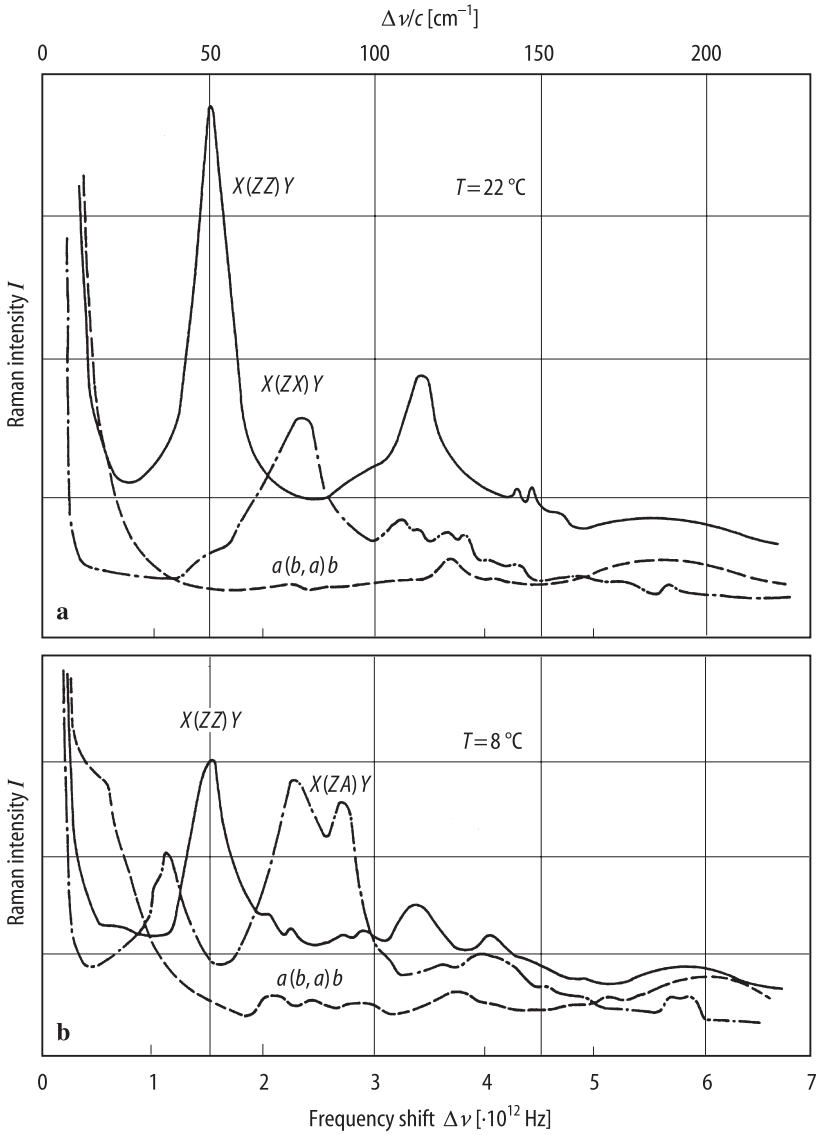

Fig. 41A-5-039. NH_4LiSO_4. I vs. $\Delta\nu$ [77Pou]. I: Raman scattering intensity for various scattering geometries. $\Delta\nu$: frequency shift. (**a**) $T > \Theta_{III-II}$, (**b**) $T < \Theta_{III-II}$.

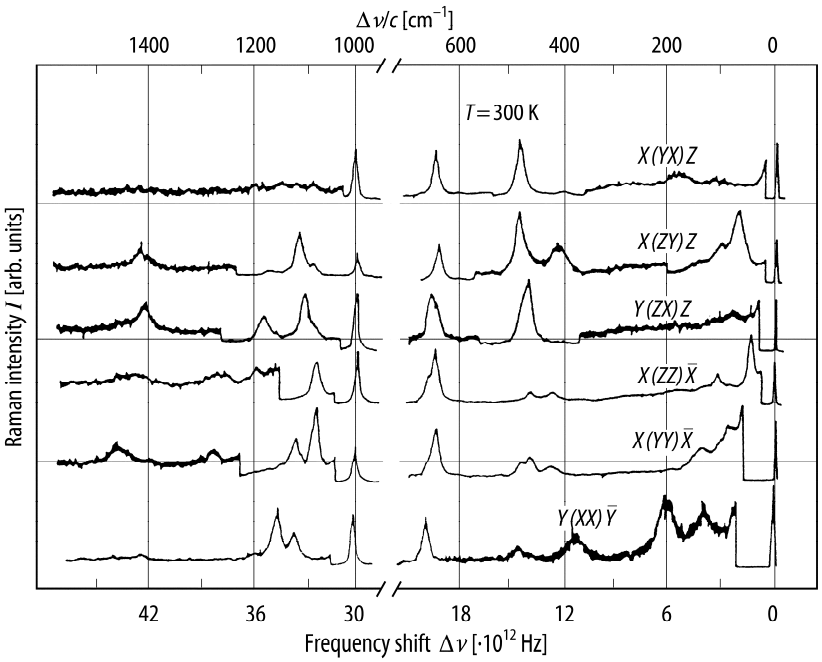

Fig. 41A-5-040. NH_4LiSO_4. *I* vs. $\Delta\nu$ [89Lem]. *I*: Raman scattering intensity at 300 K. Parameter: scattering geometry.

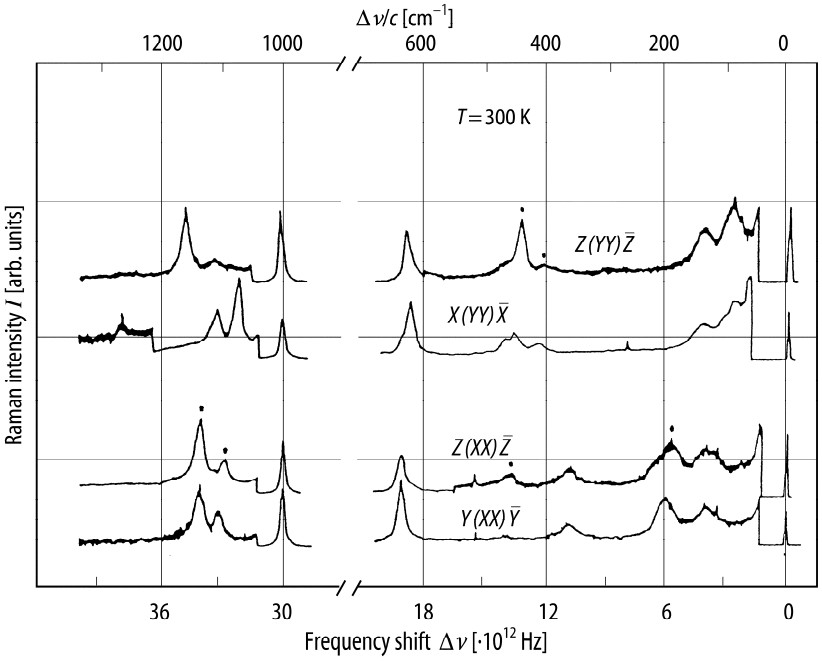

Fig. 41A-5-041. NH_4LiSO_4. *I* vs. $\Delta\nu$ [89Lem]. *I*: Raman scattering intensity of A_1 mode at 300 K. Parameter: scattering geometry.

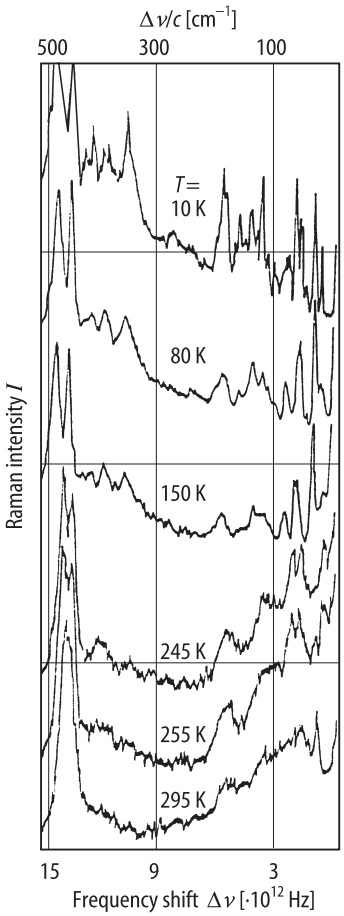

Fig. 41A-5-042. NH_4LiSO_4. I vs. $\Delta\nu$ [89Chh]. I: Raman scattering intensity. Parameter: T.

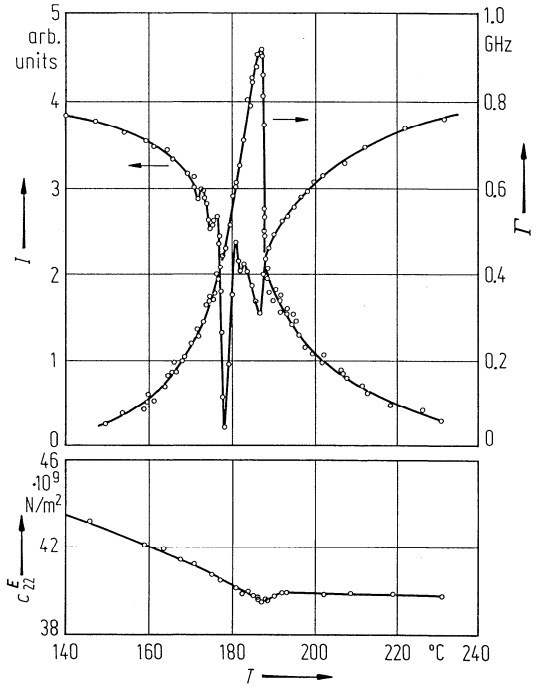

Fig. 41A-5-043. NH_4LiSO_4. c_{22}^E, I, Γ vs. T [84Lus]. I: Brillouin scattering intensity of the acoustic mode propagating along the b axis. Γ: full line width at half maximum of the Brillouin scattering spectra.

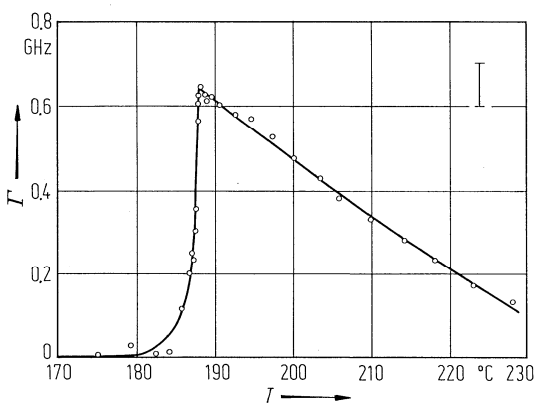

Fig. 41A-5-044. NH_4LiSO_4. Γ vs. T [85Lus]. Γ: full line width at half maximum of the Brillouin scattering spectra corresponding to $(c_{55} + c_{66})/2$.

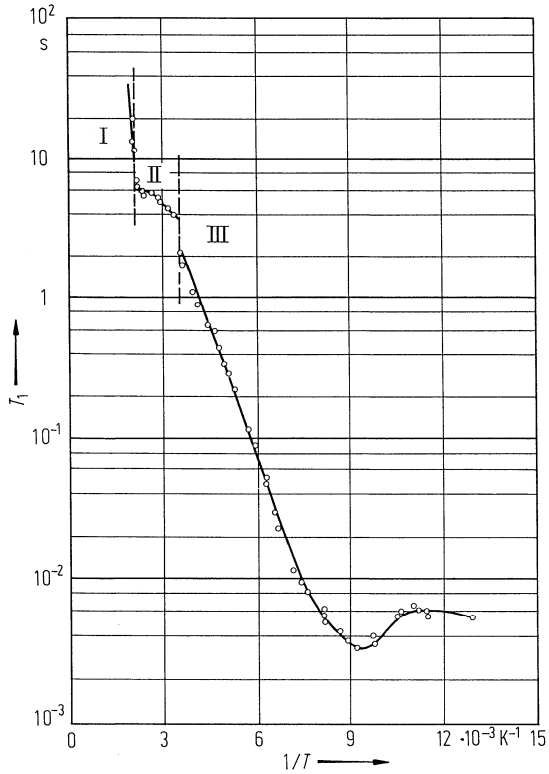

Fig. 41A-5-045. NH_4LiSO_4. Proton T_1 vs. $1/T$ [80She]. f = 10 MHz.

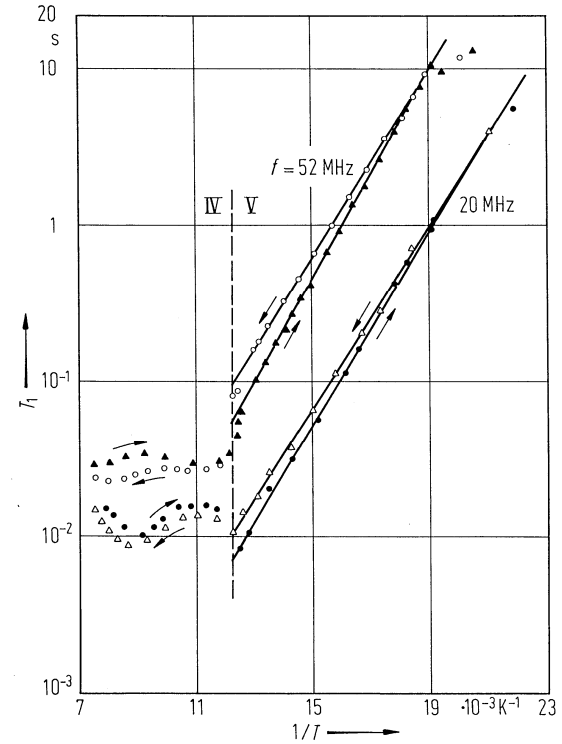

Fig. 41A-5-046. NH_4LiSO_4. Proton T_1 vs. $1/T$ [82Rey]. Parameter: f.

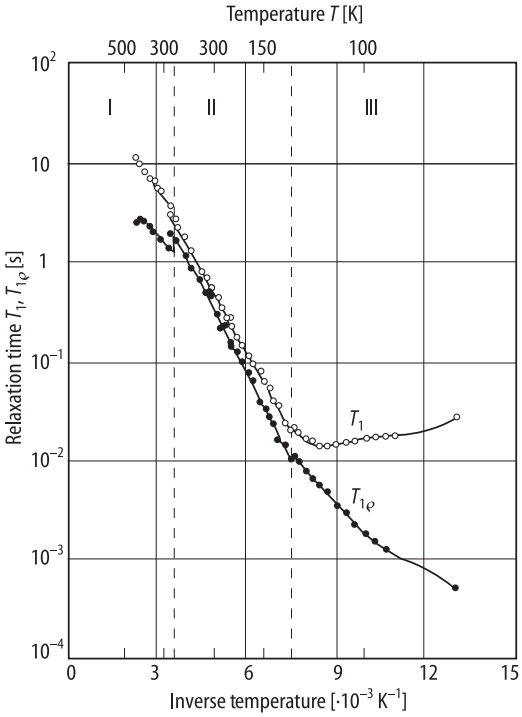

Fig. 41A-5-047. NH_4LiSO_4. T_1, $T_{1\rho}$ vs. $1/T$ [78Wat]. T_1: proton spin-lattice relaxation time. $T_{1\rho}$: proton spin-lattice relaxation time in the rotary frame. $H_1 = 1.19 \cdot 10^3$ A m^{-1}.

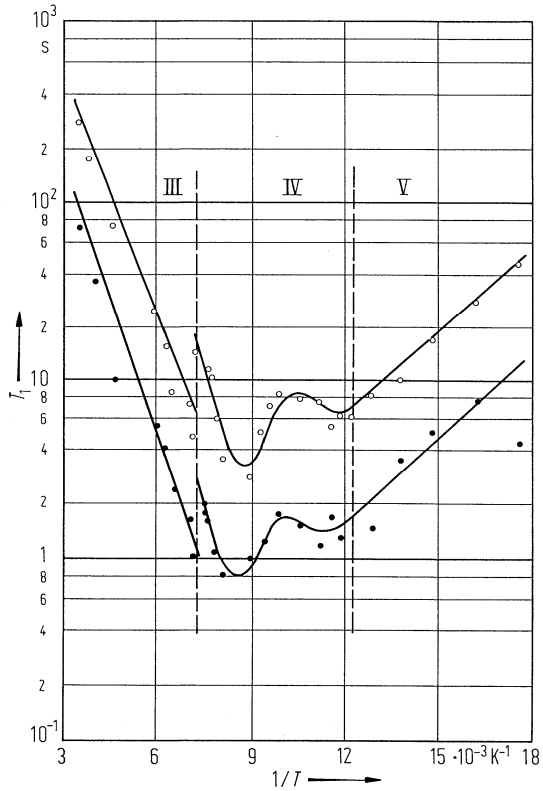

Fig. 41A-5-048. NH_4LiSO_4. ^{7}Li T_1 vs. $1/T$ [82Rey]. T_1: spin-lattice relaxation time. $f = 30$ MHz. Open circle: longer T_1, full circle: shorter T_1.

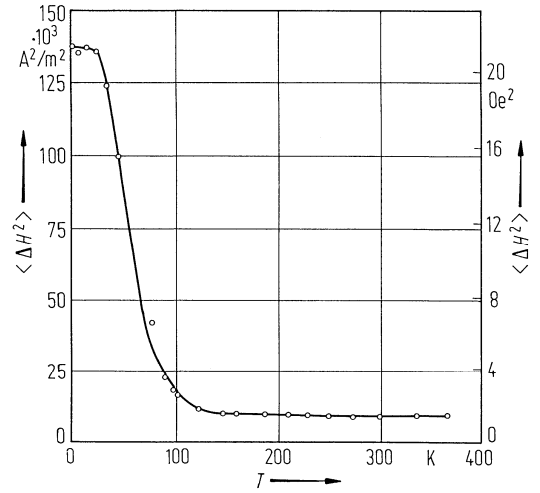

Fig. 41A-5-049. NH_4LiSO_4. Proton second moment vs. T [82Rey].

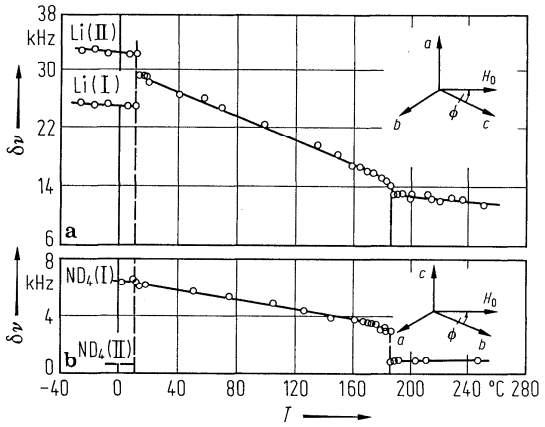

Fig. 41A-5-050. ND_4LiSO_4. $\delta\nu$ vs. T [77Ale1]. $\delta\nu$: quadrupole splitting. (**a**) ^{7}Li, $\phi = 14°$. (**b**) ^{2}D, $\phi = 45°$.

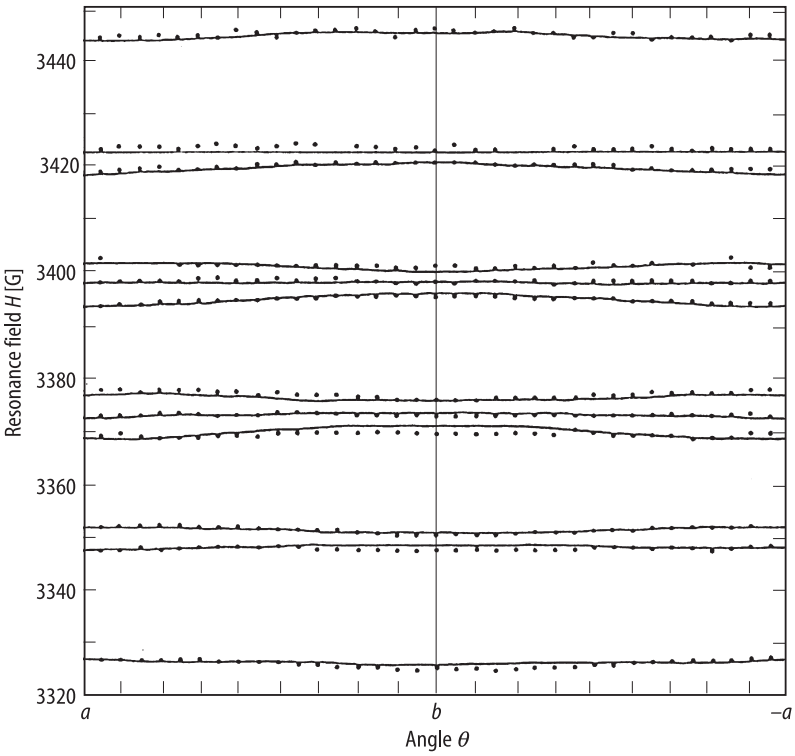

Fig. 41A-5-051. NH_4LiSO_4. H vs. θ [88Tsa]. T = RT. H: electric paramagnetic resonance field of NH_3^+ in the *ab* plane.

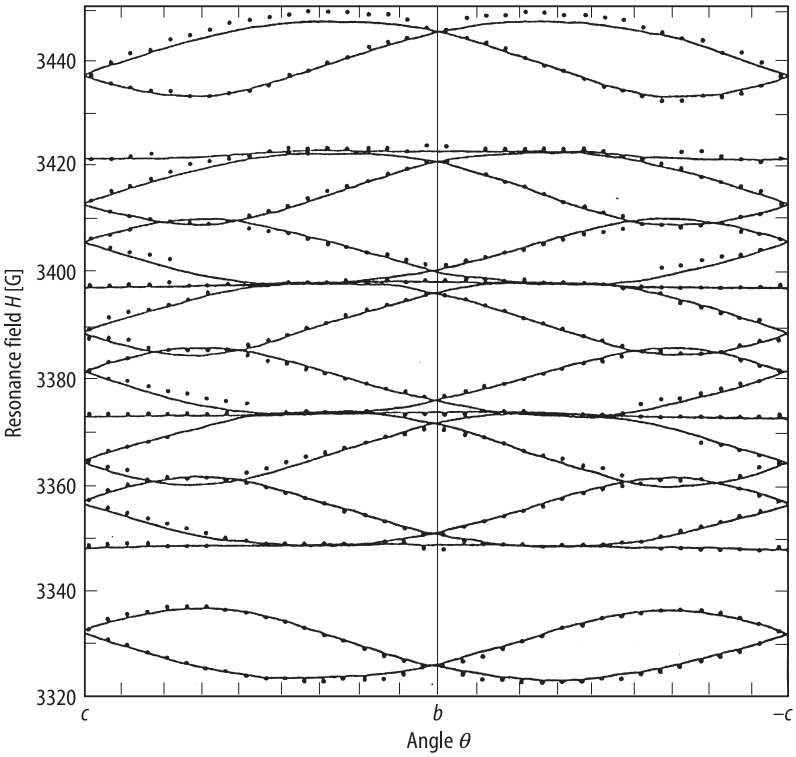

Fig. 41A-5-052. NH_4LiSO_4. H vs. θ [88Tsa]. T = RT. H: electric paramagnetic resonance field of NH_3^+ in the *bc* plane.

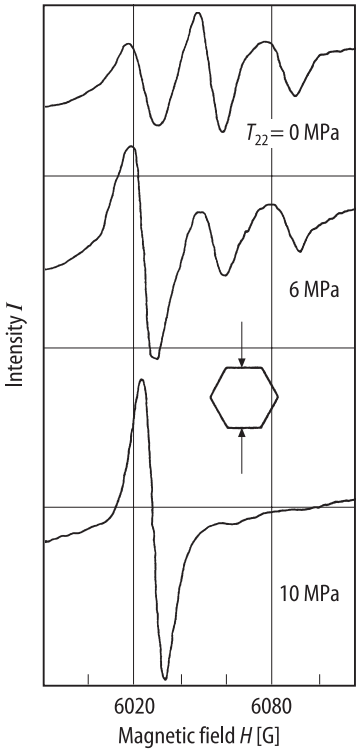

Fig. 41A-5-053. NH_4LiSO_4. I vs. H [88Tsa]. I: intensity of electric paramagnetic resonance line in phase V. $H_0 \parallel a$. Parameter: T_{22}. T_{22}: uniaxial compression stress along the b axis, indicated in insert.

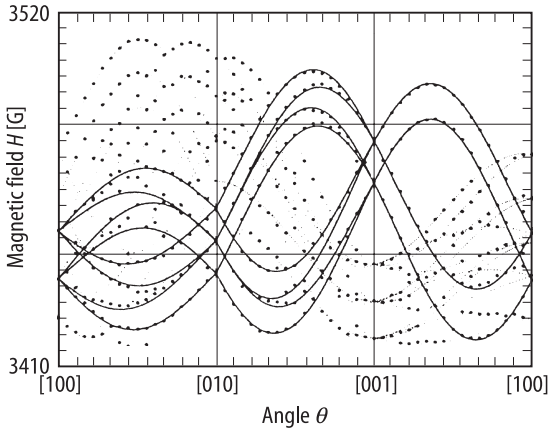

Fig. 41A-5-054. NH_4LiSO_4. H vs. θ [93Cho]. T = RT. H: resonance field of EPR line of CrO_4^{3-}. θ: angle between crystal axes and H_0.

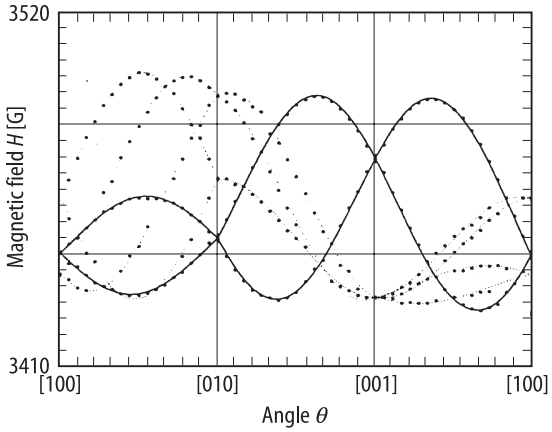

Fig. 41A-5-055. ND_4LiSO_4. H vs. θ [93Cho]. T = RT. H: resonance field of EPR line of CrO_4^{3-}. θ: angle between crystal axes and H_0.

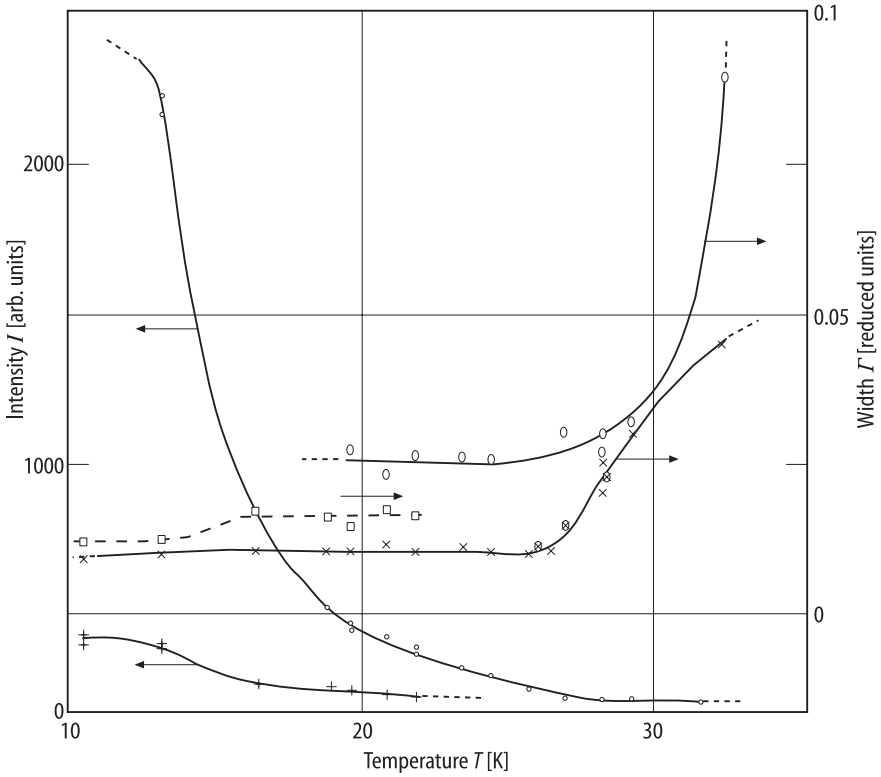

Fig. 41A-5-056. NH_4LiSO_4. I, Γ vs. T [84Sim]. I: intensity of (1/2 1/2 $\bar{7}$) (small circle) and (3/2 3/2 $\bar{9}$) (plus). Γ: width of (1/2 1/2 $\bar{7}$) on heating along $\boldsymbol{a}^*/2 + \boldsymbol{b}^*/2$ (large circle), along $\boldsymbol{c}^*$ (cross) and on cooling along c (crossed circle). Width of (3/2 3/2 $\bar{9}$) along $\boldsymbol{a}^*/2 + \boldsymbol{b}^*/2$ (open square). The unit widths are $|\boldsymbol{a}^*/2 + \boldsymbol{b}^*/2| = 1.38$ Å^{-1} and $|\boldsymbol{c}^*| = 0.73$ Å^{-1}, respectively. The widths at 10 K are the instrumental resolution.

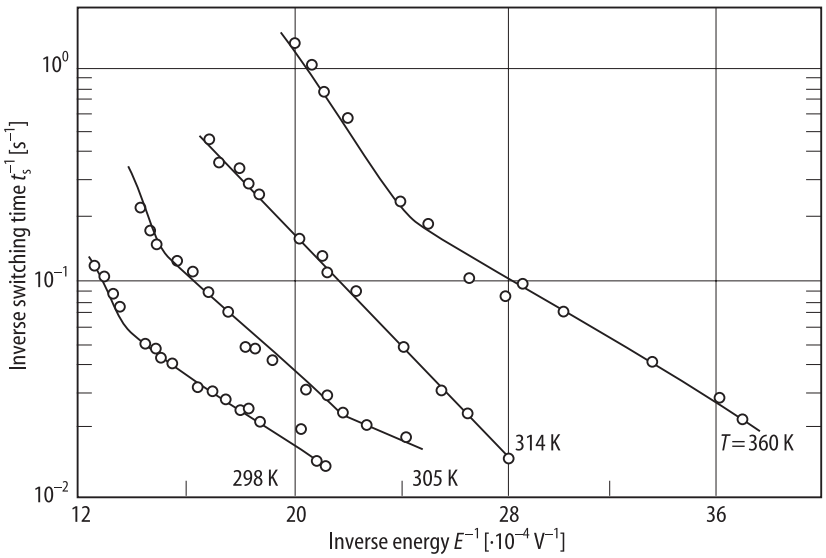

Fig. 41A-5-057. NH_4LiSO_4. $1/t_s$ vs. $1/E$ [92Pol]. Parameter: T. t_s: domain switching time.